

Continuously Learning to Detect People on the Fly: A Bio-inspired Visual System for Drones

Ali Safa, *Student Member, IEEE*, Ilja Ocket, *Member, IEEE*, André Bourdoux, *Senior Member, IEEE*,
Hichem Sahli, Francky Catthoor, *Fellow, IEEE*, Georges G.E. Gielen, *Fellow, IEEE*

Abstract—This paper demonstrates for the first time that a biologically-plausible spiking neural network (SNN) equipped with Spike-Timing-Dependent Plasticity (STDP) can continuously learn to detect walking people on the fly using retina-inspired, event-based cameras. Our pipeline works as follows. First, a short sequence of event data (< 2 minutes), capturing a walking human by a flying drone, is forwarded to a convolutional SNN-STDP system which also receives teacher spiking signals from a readout (forming a semi-supervised system). Then, STDP adaptation is stopped and the learned system is assessed on testing sequences. We conduct several experiments to study the effect of key parameters in our system and to compare it against conventionally-trained CNNs. We show that our system reaches a higher peak F_1 score (+19%) compared to CNNs with event-based camera frames, while enabling on-line adaptation.

Index Terms—Bio-inspired vision, continual learning, drones

I. INTRODUCTION

IN recent years, the use of micro drones has attracted much attention for applications ranging from infrastructure inspection to people search and rescue [1]. In those applications, drones and humans will be moving within the same environment. Therefore, it is critical to equip micro drones with people detection pipelines for safety purposes [2].

Following the enormous progress in *deep learning*, convolutional neural networks (CNNs) such as *You Only Look Once* (YOLO) and its variants, constitute the state of the art in terms of detection and speed performance [3]. However, the use of such CNNs is not suited for micro drones because of the significant power budget that conventional CNNs demand (2W for an edge TPU, 10W for a Jetson Nano) relative to the micro drone power budget (< 1 W). Therefore, a significant effort has been put in the co-design of CNNs and micro-controller (MCU) architectures in order to reduce the power and memory consumption budget of the vision system down to < 100 mW and < 1 MB respectively [4]. Still, adopting a conventional CNN-hardware design approach leads to rigid systems that cannot easily adapt themselves to new environments and tasks (unlike the nervous systems of biological entities in nature).

Indeed, conventional CNNs rely on the standard off-line training procedure where the CNN is trained on a large dataset capturing the task that needs to be solved. However, it is not always guaranteed that all scenarios to be encountered at run time are well captured by the training set (e.g., partially

A. Safa, I. Ocket, F. Catthoor and G. G.E Gielen are with imec and KU Leuven, 3001 Leuven, Belgium (Ali.Safa-Ilja.Ocket-Francky.Catthoor@imec.be; Georges.Gielen@kuleuven.be). A. Bourdoux is with imec, 3001 Leuven, Belgium (Andre.Bourdoux@imec.be). H. Sahli is with imec and ETRO VUB, 1050 Brussels, Belgium (hsahli@etrovub.be)

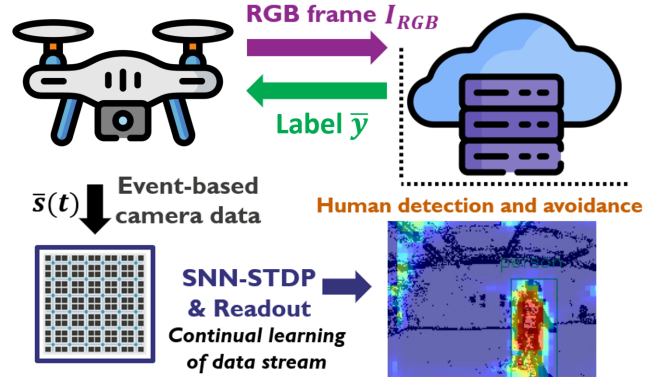


Fig. 2: *Continual learning of people detection.* Conceptual illustration of a micro-drone equipped with an event-based camera, an RGB camera and a bio-inspired SNN-STDP network. The RGB frames are sent to a back-end server where an oracle CNN returns people detection labels. The labels are used during the continual learning of the SNN-STDP system.

damaged infrastructures are hard to capture by a dedicated dataset for *indoor search and rescue* tasks). In addition, since CNN training requires desktop-grade computing, the conventional solution for fine-tuning on-board CNNs is to first re-train the network offline and then send the updated weights back to the drone. Clearly, this conventional approach has many drawbacks such as high latency (training takes a long time, prohibiting fast adaptation) and privacy concerns due to the on-line storage of user data (also causing legal issues due to e.g., the *right to data erasure* in the EU¹).

Recently, the use of biologically-inspired *spiking neural networks* (SNNs) has gained huge interest for the design of ultra-low-power AI-enabled systems [6], [12]. In contrast to CNNs, SNNs make use of spiking neurons that communicate through low-complexity binary activations in an *event-based* manner (vs. frame-based processing in CNNs), only consuming energy when a spike is emitted [12]. In addition, SNNs can be implemented in massively parallel, *non Von Neumann* computing architectures, solving the energy- and latency-expensive memory bottleneck issues [6]. Finally, the use of a bio-inspired learning rule (vs. backprop) working in the binary activation domain and *local* to each neuron (such as *Spike-Timing-Dependent Plasticity* or STDP [8]) enables ultra-low-power learning at the edge (not tackled by embedded CNNs) [9]. Therefore, a growing number of SNN-STDP computing

¹<https://gdpr.eu/right-to-be-forgotten/>

units have been proposed, achieving a power consumption as low as $\sim 100\mu\text{W}$ [9] while enabling *on-chip inference and learning* (three orders of magnitude lower power consumption vs. optimized CNNs running on MCU [4]).

As SNNs require spiking data as input, they are often used in conjunction with an *event-based camera* (also called *dynamic vision sensor* or DVS), inspired by the inner working of the human eye. DVS cameras are composed of independent pixels that emit spikes asynchronously whenever the change in light log-intensity crosses a threshold C [10] (see Fig. 1).

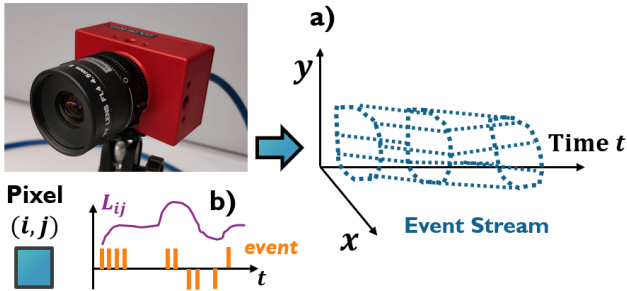


Fig. 1: **Conceptual illustration of event-based data.** The DVS is capturing an image of “0”. a) The DVS outputs a spike stream in time and space. b) When the change $|\Delta L_{ij}|$ in light L_{ij} at pixel (i, j) crosses a threshold C , a spike is emitted. The spike is positive if $\Delta L_{ij} > 0$ and negative otherwise.

In this paper, our goal is to investigate the design of a bio-inspired SNN-STDP system that can *continuously learn* to perform people detection on drones from DVS camera data. Fig. 2 illustrates the scenario that we consider in this work: the drone must explore the environment during ~ 2 minutes and continuously learn to detect a walking human subject using the current data sample only, *without access to the past and the future data*. Then, continual learning (CL) is stopped and we assess the detection performance on a testing sequence.

As the basis for our people detection network, we use the state-of-the-art SNN-STDP architecture proposed in [12] and we augment it with three significant enhancements: *i*) we motivate and extend the SNN-STDP network to the use of *anti-Hebbian* (negative STDP) learning rules; *ii*) we propose a semi-supervised method that allows the learning of the logistic regression readout and the SNN *at the same time* (vs. disjoint learning in [12]) and *iii*) we use our SNN in a more challenging CL setting (vs. offline training in [12]).

This paper is organized as follows. Related works are discussed in Section II. Background theory is given in Section III. Our methods are presented in Section IV. Results are discussed in Section V. Conclusions are given in Section VI.

II. RELATED WORKS

A growing number of bio-inspired robotic systems have been proposed in the past decades, mainly focusing on the study of animal-like actuation and motor control [11]. Complementary to bio-actuation, a number of perception systems for drones, taking inspiration from the inner workings of the human eye and the visual cortex, have recently emerged thanks to the advent of neuromorphic event-based cameras [6], [7],

[10]. A line tracking system for drones was proposed in [6] using a DVS camera processed by an SNN. Similar to our work, the system of [6] uses an SNN with local bio-inspired learning rules (analogous to STDP) and demonstrates that such adaptive SNN system can learn to compensate for external disturbances online. Closer to our work, a DVS-based moving object tracking system for drones was proposed in [7], using hand-crafted feature extraction followed by Kalman filtering (processing pipeline not bio-plausible). Compared to the hand-crafted feature extraction in [7], we proposed a bio-inspired vision system that can continuously *learn* to detect walking people from a drone (vs. detecting *any* moving object in [7]).

Since sparsely-supervised and unsupervised learning are believed to be key mechanisms in the brain, a number of bio-inspired architectures have been proposed for learning spatio-temporal features from event-based data [12], [18]. Among them, the *hierarchy of event-based time surfaces* (HOTS) was proposed in [18] by cascading unsupervised layers, trained to cluster event-data aggregated as *time surfaces* (exponential decay maps) and by using an output readout (e.g., logistic regression) to classify the extracted features. In contrast to HOTS, which uses conventional clustering methods, an unsupervised SNN-STDP network with better biological plausibility was proposed by us in [12] for DVS feature learning, achieving state-of-the-art performance on common DVS benchmarks. Thus, we use the network of [12] as our basis in this work.

III. BACKGROUND THEORY

A. SNN-STDP fundamentals

In contrast to CNNs, SNNs make use of *spiking* neurons, often modelled by a Leaky Integrate-and-Fire (LIF) activation:

$$\begin{cases} \frac{dV}{dt} = \frac{1}{\tau_m} (J_{in} - V) \\ \sigma = 1, V \leftarrow 0 \text{ if } V \geq \mu, \text{ else } \sigma = 0 \end{cases} \quad (1)$$

with J_{in} the input current to the neuron, σ the spiking output, V the membrane potential, τ_m the membrane time constant and μ the neuron threshold [12]. The scalar input current J_{in} is continuously integrated in V following (1). When V crosses the firing threshold μ , the membrane potential is reset back to zero and an output spike is emitted. The input current J_{in} is obtained by filtering the inner product of the neural weights and the spiking inputs through a *post-synaptic current* (PSC) kernel [12] (estimating the spiking rate):

$$J_{in} = \mathcal{PSC}\{\bar{w}^T \bar{s}_{in}(t)\} \quad (2)$$

with $\bar{s}_{in}(t)$ the input spiking vector (originating from e.g. an event camera or other spiking neurons), \bar{w} the weight vector and $\mathcal{PSC}\{\theta(t)\} = \theta(t) * \frac{1}{\tau_s} e^{-t/\tau_s}$ the effect of PSC filtering with time constant τ_s . Fig. 3 a) conceptually illustrates the LIF neuron behaviour. In the SNN architecture used in this work, learning is performed using the STDP rule, *locally* modifying the weights w_{ij} of each neuron i as follows:

$$w_{ij} \leftarrow \begin{cases} w_{ij} + A_+ e^{-\tau_{ij}/\tau_+}, & \text{if } \tau_{ij} \geq 0 \\ w_{ij} - A_- e^{\tau_{ij}/\tau_-}, & \text{if } \tau_{ij} < 0 \end{cases} \quad (3)$$

with A_+ , A_- the long-term potentiation (LTP) and depression (LTD) weights, τ_+ , τ_- the potentiation and depression decay

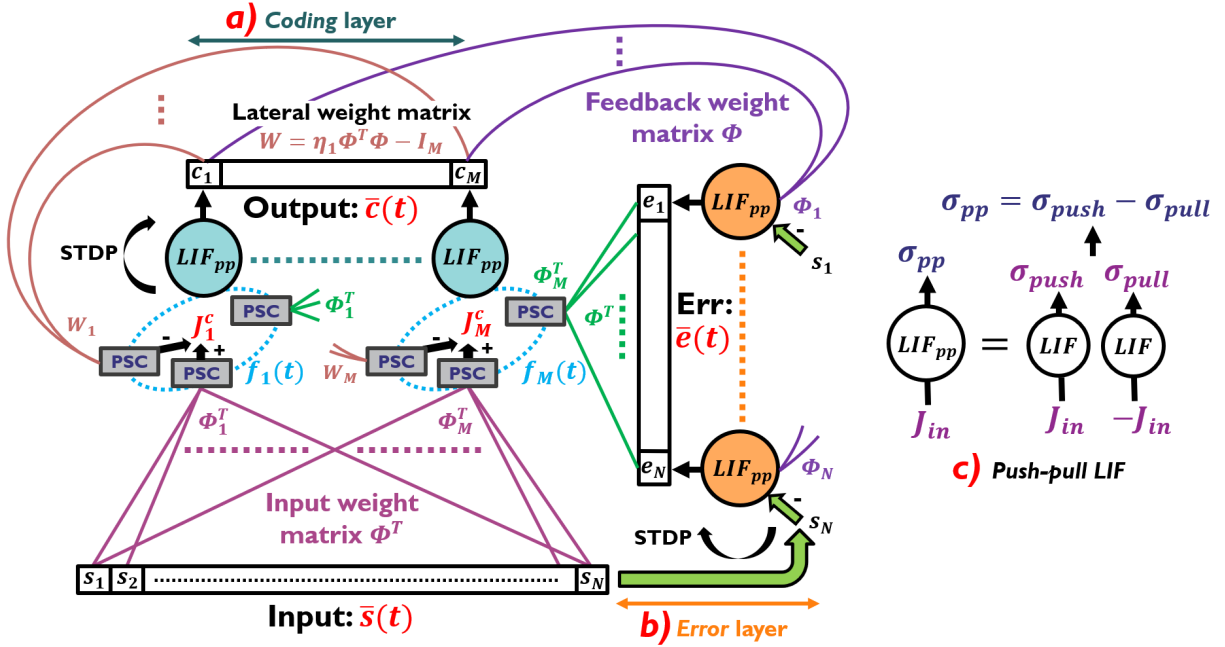


Fig. 4: **SNN-STDP architecture.** a) The coding layer features $i = 1, \dots, M$ pairs of push-pull LIF neurons (LIF_{pp}) that receive the spiking vector \bar{s} (input) through Φ^T (input weights) and the previous spiking output vector \bar{c} through W (lateral weights). The output spike trains \bar{c} are obtained following (7). In addition, the coding layer receives the re-projection error spike trains \bar{e} through Φ^T and combines them with the other inputs using (8) to obtain f_i locally to each coding neuron. STDP is applied for learning Φ^T and W with c_i and f_i the post-synaptic and \bar{e} the pre-synaptic spike trains. b) The error layer features $j = 1, \dots, N$ pairs of push-pull LIF neurons LIF_{pp} which receive the entry s_j as input and the SNN output \bar{c} through Φ (feedback weights, remain identical to the transpose of input weights during learning). The error layer outputs the spiking vector \bar{e} following (6). STDP is applied for learning Φ with each $e_j(t)$ as the post-synaptic spike train and \bar{c} as the pre-synaptic spike trains. c) The pair of push-pull LIF neurons codes both positive and negative values of the input current J_{in} (output spikes of positive or negative polarity).

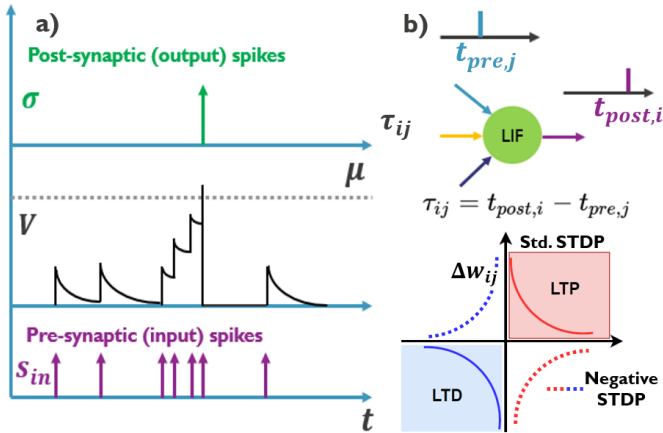


Fig. 3: **Conceptual illustration of the LIF neuron and STDP learning.** a) The LIF receives as input a pre-synaptic spike train s_{in} . When the LIF membrane potential V rises above the threshold μ , a spike is emitted ($\sigma = 1$) and V is set back to zero. b) The synapse strength is modified following the double exponential STDP rule (3) in function of the difference between the post- and the pre-synaptic spike times $\tau_{ij} = t_{post,i} - t_{pre,j}$.

constants, w_{ij} the j^{th} element of the i^{th} neuron weight vector \bar{w} and τ_{ij} the time difference between the post- and the pre-synaptic spike times across the j^{th} synapse of neuron i (see Fig. 3 b) [8]. Finally, it can be shown [12] that a good approximation for the long-term effect of STDP (i.e., its expected value over time t) is given by the product of the post- and pre-synaptic mean spike rates (noted $r_{post,pre}$):

$$\Delta w_{STDP}\{s_{post}, s_{pre}\} \approx \eta_2 (A_+ \tau_+ - A_- \tau_-) r_{post} r_{pre} \quad (4)$$

where η_2 is the learning rate.

B. SNN-STDP as Dictionary Learning, Basis Pursuit (DLBP)

As proposed in [12], the SNN-STDP in Fig. 4 is iteratively solving the *unsupervised* DLBP problem (inferring \bar{c} using the current Φ and learning the next Φ using the current \bar{c}):

$$\bar{c}, \Phi = \arg \min_{\bar{c}, \Phi} \frac{1}{2} \|\Phi \bar{c} - \bar{s}\|_2^2 + \lambda_1 \|\bar{c}\|_1 + \frac{\lambda_2}{2} \|\Phi\|_F^2 \quad (5)$$

where \bar{c} is the M -dimensional output vector containing the mean spike rates of each output neuron in the SNN, Φ is the learned network weight matrix, \bar{s} is the N -dimensional input vector, λ_1 is a sparsity-controlling hyper-parameter and λ_2 is a weight decay hyper-parameter.

DLBP (5) is solved iteratively by applying STDP across all neurons as follows [12]. The j^{th} neuron in the error layer

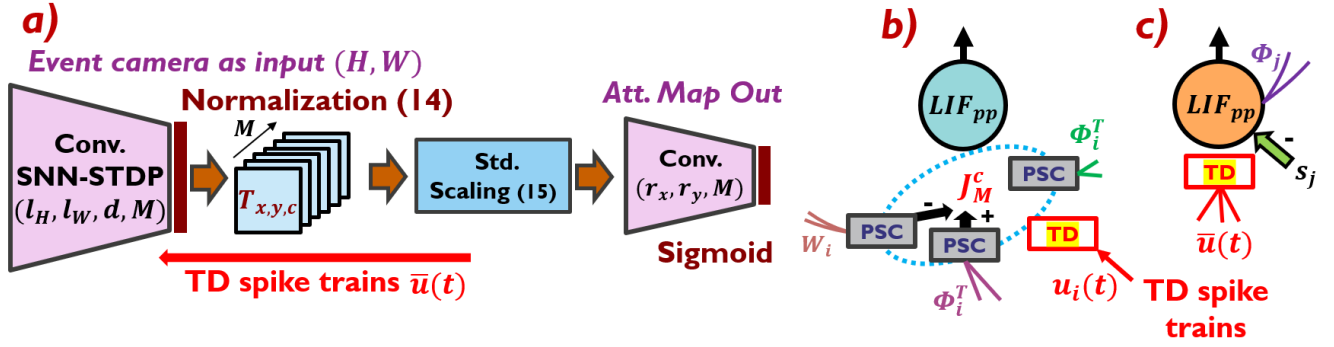


Fig. 5: *Network architecture for CL and people detection using a DVS camera.* a) Convolutional SNN-STDP followed by a convolutional readout layer. The SNN output is normalized using (14). The normalized tensor is then fed to a standard scaling block (15) and the resulting tensor is processed by the readout. The readout outputs an attention map indicating the position of a human subject on the image plane. The readout continuously outputs a task-driven (TD) signal $\bar{u}(t)$ following (23). b) The i^{th} neuron in the coding layer (see Fig. 4 a) is augmented with an additional synapse to receive the i^{th} component of the TD signal $u_i(t)$. c) The j^{th} neuron in the error layer (see Fig. 4 b) is augmented with additional inputs receiving $\bar{u}(t)$.

(see Fig. 4 b) receives as input the spike trains from the coding layer and outputs the reconstruction error in the spike domain:

$$e_j = LIF_{pp}\{\Phi_j \bar{c} - s_j\} \quad (6)$$

where Φ_j is locally modified by applying STDP with the e_j as the post- and $\bar{c}(t)$ as the pre-synaptic spike trains. LIF_{pp} denotes the application of a push-pull pair of LIF neurons (1) (see Fig. 4 c). The i^{th} neuron in the coding layer (see Fig. 4 a) receives \bar{s} and the *previous* output vector \bar{c} as input, and generates the output (where Φ_i, W_i are the i^{th} matrix rows):

$$c_i = LIF_{pp}\{\Phi_i \bar{s} - W_i \bar{c}\}, \quad W \equiv \eta_1 \tilde{W} - I_M, \quad \tilde{W} \equiv \Phi^T \Phi \quad (7)$$

with η_1 the output convergence rate (to be set) and I_M the identity matrix of dimension M . Each coding neuron i also receives the error vector \bar{e} from the error layer and locally combines it with its inputs \bar{c} and \bar{s} to form the local signal f_i :

$$f_i(t) = \underbrace{\eta_1^{-1}(W + I_M)_i}_{\tilde{W}_i(7)} \bar{c}(t) - (\Phi^T)_i \bar{e}(t) - (\Phi^T)_i \bar{s}(t) \quad (8)$$

$$\approx (\tilde{W} - \Phi^T \Phi)_i \bar{c}(t)$$

Then, STDP is applied across each neuron i using c_i as the post- and \bar{e} as the pre-synaptic spike trains for learning Φ^T . STDP is also applied using f_i as the post- and \bar{e} as the pre-synaptic spike trains for learning W [12]. Finally, it can be remarked that the SNN-STDP architecture of Fig. 4 can naturally be extended to the *convolutional* setting by sweeping the network of Fig. 4 across a $H \times W$ image plane with kernel size $[l_x, l_y]$ and stride d [12]. A spiking tensor of dimension:

$$[D_x, D_y, D_c] = \left[\frac{H - l_x}{d} + 1, \frac{W - l_y}{d} + 1, M \right] \quad (9)$$

is obtained. In this convolutional case, (5) can keep a similar form by considering Φ as a *circulant* matrix and $\bar{s}, \bar{c}, \bar{e}$ as flattened tensors along the image plane dimension.

IV. PROPOSED METHODS

A. Extension to anti-Hebbian learning

Anti-Hebbian learning (or negative STDP, see Fig. 3 b) refers to the application of the *opposite* of the STDP rule

(3) with *negative* A_+ and A_- quantities in (3), and has been investigated in a few works [13]. Following the derivations in [12], it can be shown that using *negative STDP* for learning the input weights Φ^T and feedback weights Φ (see Fig. 4), while using *standard STDP* for the learning of the lateral weights W (7), the following *joint* optimisation objective is solved:

$$\begin{cases} \bar{c} = \arg \min_{\bar{c}} \|\Phi \bar{c} - \bar{s}\|_2^2 + \lambda_1 \|\bar{c}\|_1 \\ \Phi = \arg \min_{\Phi} -\log(\|\Phi \bar{c} - \bar{s}\|_2^2) + \frac{\lambda_2}{2} \|\Phi\|_F^2 \end{cases} \quad (10)$$

Similar to (5), the SNN iterations infer the next SNN output \bar{c} by considering the current Φ constant and learns the next SNN weight matrix Φ by considering the current \bar{c} fixed.

Negative STDP solves (10) since:

$$\frac{\partial}{\partial \Phi} \{-\log(\|\Phi \bar{c} - \bar{s}\|_2^2)\} = -\frac{(\Phi \bar{c} - \bar{s}) \bar{c}^T}{\|\Phi \bar{c} - \bar{s}\|_2^2} \quad (11)$$

and since it has been shown in [12] that *standard* STDP approximates the gradient-based learning:

$$\Phi \leftarrow \Phi - \eta_2 (\Phi \bar{c} - \bar{s}) \bar{c}^T - \eta_2 \lambda_2 \Phi \quad (12)$$

it is now clear that *negative* STDP approximating:

$$\Phi \leftarrow \Phi - \eta_2 \{-(\Phi \bar{c} - \bar{s}) \bar{c}^T\} - \eta_2 \lambda_2 \Phi \quad (13)$$

is using a gradient similar to (11) (up to a dividing scalar oscillating around ~ 100 during our experiments) and is learning Φ in (10). When combined with a *supervision term* (see Section IV-C), the use of the *negative* STDP rule can be motivated as a *regularization* controlling the over-fitting of the SNN-STDP by preventing the re-projection $\|\Phi \bar{c} - \bar{s}\|_2^2$ from becoming too small (see experiments in Section V-B).

B. Proposed bio-inspired SNN-STDP architecture

Fig. 5 a) shows the CL SNN-STDP system used throughout this work to infer attention maps. We set up a convolutional network by cascading the SNN-STDP network of Section IV-A (in a convolutional setting with *negative* STDP learning) with a convolutional readout in order to learn attention maps. At the

output of the convolutional readout, we use *sigmoid* activation functions in order to constrain the dynamic range of the attention map between 0 and 1. The rate of the spiking activity at the SNN output is estimated using a rolling time window of length $N_s = 20$. Doing so, a tensor $T_{x,y,c}$ containing the mean spike rates for each spatial coordinate $[x, y]$ and each channel c is obtained. Then, $T_{x,y,c}$ is normalized along the channel dimension c to provide invariance to event density [12]:

$$\tilde{T}_{x,y,c} = \frac{|T_{x,y,c}|}{\sum_c |T_{x,y,c}|} \quad (14)$$

In between the SNN-STDP layer and the readout, we use *standard scaling* along the channel dimension c in order to reduce the internal covariate shifts [14]:

$$T_{x,y,c}^* = \frac{\tilde{T}_{x,y,c} - \mu_c}{\sigma_c} \quad (15)$$

where the mean μ_c and standard deviation σ_c are estimated on-line. We note the transformations (14)(15) of \bar{c} into T^* as $T^*\{\bar{c}\}$. Finally, $T_{x,y,c}^*$ is *zero-padded* and fed to the readout layer with a convolutional kernel size $[r_x, r_y, M]$ in order to obtain an attention map $A_{x,y}$ of dimension $[D_x, D_y]$ following (9). Finally, we interpolate the attention map $A_{x,y}$ back to the input size $[H, W]$.

Without the use of the normalization mechanisms (14)(15), we observed the CL process to fail due to the severe covariate shifts encountered during learning. In addition, we observed that using a convolutional readout layer over a standard fully-connected layer is crucial in order to avoid readout *overfitting* on the local context encountered by the drone during the CL process (CL fails when using a fully-connected layer). The architecture of Fig. 5 a) also shows that the readout generates a vector of *task-driven* (TD) spike trains $\bar{u}(t)$ that is fed back to the SNN neurons. The TD spike trains are used to *steer* the unsupervised STDP-driven weight dynamics in order to *jointly* optimize the SNN weights Φ and the readout Ψ , forming a task-driven, semi-supervised learning system.

C. Task-driven semi-supervised learning

During our experiments, we observe that the SNN-STDP system and the readout should not be optimised independently as in [12] (i.e., *unsupervised* learning of SNN and *disjoint* learning of a readout). Rather, the SNN and the readout must be learned concurrently. Indeed, if the learning process would be independent, the way the readout should fit the SNN output in the beginning of the STDP learning process will not be the same as in the end, since the SNN weights have *independently* changed since then, leading to significant covariate shifts at the input of the readout. Following this discussion, and the effectiveness of unsupervised DVS learning [12], we opt for a *joint* semi-supervised SNN-readout objective:

$$\begin{cases} \bar{c} = \arg \min_{\bar{c}} \|\Phi \bar{c} - \bar{s}\|_2^2 + \lambda_1 \|\bar{c}\|_1 \\ \Phi = \arg \min_{\Phi} \lambda_s \mathcal{L}_{sup}(\bar{\sigma}(\Psi, T^*\{\bar{c}\}, \bar{b}), \bar{y}) \\ \quad - \lambda_u \log(\|\Phi \bar{c} - \bar{s}\|_2^2) + \frac{\lambda_2}{2} \|\Phi\|_F^2 \\ \Psi = \arg \min_{\Psi} \lambda_s \mathcal{L}_{sup}(\bar{\sigma}(\Psi, T^*\{\bar{c}\}, \bar{b}), \bar{y}) \end{cases} \quad (16)$$

where in addition to (10), Ψ is the $K \times M$ weight matrix of the readout, \bar{b} the learned bias vector, $\sigma(\cdot)$ the sigmoid activation,

\bar{y} the desired output label vector of dimension $K \times 1$, \mathcal{L}_{sup} the supervised loss function and $\lambda_{u,s}$ the hyper-parameters controlling the strength of the unsupervised and supervised contributions. As usual, the network infers the next \bar{c} keeping Φ, Ψ constant, then learn Φ keeping Ψ, \bar{c} constant and so on. We choose \mathcal{L}_{sup} as the *focal loss* because of its robustness to imbalanced data compared to the standard cross-entropy [15]:

$$\mathcal{L}_{sup}(\sigma_i(\Psi_i, T^*\{\bar{c}\}, \bar{b}), y_i) = -(1 - p_i)^\gamma \log(p_i) \quad (17)$$

with γ setting the robustness to class imbalance and:

$$p_i = \begin{cases} \sigma_i(\Psi_i, T^*\{\bar{c}\}, \bar{b}) & \text{if } y_i = 1 \\ 1 - \sigma_i(\Psi_i, T^*\{\bar{c}\}, \bar{b}) & \text{otherwise} \end{cases} \quad (18)$$

In order to optimise \mathcal{L}_{sup} as a function of the SNN weights Φ , the link between \bar{c} and Φ must be made explicit. Since \bar{c} is the result of an iterative process involving the LIF neuron non-linearity, an analytical function $\bar{c}(\Phi, \bar{s})$ is hard to find and further relaxations must be done. First, we observe in (16) that for a small λ_1 , $\bar{c}(\Phi, \bar{s})$ is well approximated as:

$$\bar{c}(\Phi, \bar{s}) \sim (\Phi^T \Phi)^{-1} \Phi^T \bar{s} \quad (19)$$

Since Φ is initialized following an i.i.d. zero-mean normal distribution with standard deviation $\sigma_w = 0.01$ [12], the following relaxation holds during the early SNN-STDP learning steps (when most of the learning effect takes place):

$$\bar{c}(\Phi, \bar{s}) \sim \frac{1}{N\sigma_w^2} \Phi^T \bar{s} \quad (20)$$

Then, the gradient of \mathcal{L}_{sup} as a function of Φ is:

$$\frac{\partial \mathcal{L}_{sup}}{\partial \Phi} = k \bar{s} \left(\frac{\partial \mathcal{L}_{sup}}{\partial \bar{c}} \right)^T \quad (21)$$

where $k = \frac{1}{N\sigma_w^2}$ is a constant (dropped further on) and the gradient $\frac{\partial \mathcal{L}_{sup}}{\partial \bar{c}}$ directly follows from (14)(15)(17)(18).

D. Task-driven SNN-STDP topology

Thanks to the relaxation (20)(21), the original unsupervised SNN-STDP architecture of Fig. 4 can now be modified in order to incorporate the effect of the newly added task-driven term in (16). We observe in (21) that:

$$\bar{v} = \left(\frac{\partial \mathcal{L}_{sup}}{\partial \bar{c}} \right)^T \quad (22)$$

is a $1 \times M$ vector computed at the *readout side* (e.g., in an MCU used to post-process the SNN activity) while the *spike train* vector $\bar{s}(t)$ in (21) is already available in both the *coding* and *error* layers (see Fig. 4 a). Therefore, the TD contribution can be injected in the SNN-STDP system by first converting \bar{v} to a push-pull pair of spike trains as follows:

$$\bar{u}(t) = LIF_{pp}\{\bar{v}\} \quad (23)$$

Then, each entry u_i of $\bar{u}(t)$ can be fed to the i^{th} neuron in the *coding* layer via one additional synapse (see Fig. 5 b), and the spiking vector $\bar{u}(t)$ can be distributed to each *error* neuron via an additional set of synapses (see Fig. 5 c).

Finally, in addition to the unsupervised STDP mechanisms already present in the network of Fig. 4 to solve (5), it follows

from (4) that an additional STDP contribution must be applied to the neurons in the *error* layer as follows:

$$(\Phi_j)_i \leftarrow (\Phi_j)_i - \lambda_s \Delta w_{\text{STDP}} \{s_j(t), u_i(t)\} \quad (24)$$

with $s_j(t)$ the post- and $u_i(t)$ the pre-synaptic spike trains. An additional STDP contribution must also be applied to the neurons in the *coding* layer as:

$$(\Phi_i^t)_j \leftarrow (\Phi_i^t)_j - \lambda_s \Delta w_{\text{STDP}} \{u_i(t), s_j(t)\} \quad (25)$$

with $u_i(t)$ the post- and $s_j(t)$ the pre-synaptic spike trains. Regarding the lateral weights W , it can be shown [12] that the STDP mechanism adopted in the network of Fig. 4 automatically enforces consistency between the task-driven learning of Φ and the convergence of W (since applying STDP between $f_i(t)$ in (8) and $\bar{e}(t)$ in (6) forces W to converge to $\eta_1 \Phi^T \Phi - I_M$ in (7) [12]).

E. Continual learning strategy

For on-line labelling, we use a pre-trained YOLOv3 network [5] to detect the presence or absence of a human subject from the RGB frames that are jointly acquired with the DVS data, and to infer the bounding box coordinates $[b_{x,1}, b_{y,1}, b_{x,2}, b_{y,2}]$ (normalized to the size of the output map) indicating the location of the human subject in the image. When a human subject is present, the corresponding *label map* \bar{y} (used for the supervised contribution) is assigned with *ones* inside the bounding box region and *zeros* outside. Since there are significantly more zero-valued entries in \bar{y} , we use *median frequency balancing* [16] to help mitigate the learning imbalance in space. Therefore, we weight the readout loss as follows:

$$\mathcal{L}_{\text{sup}}(\sigma_i, y_i) \leftarrow w_i \mathcal{L}_{\text{sup}}(\sigma_i, y_i) \quad \text{with} \quad w_i = \frac{f_m}{N_{\text{class},i}} \quad (26)$$

where $N_{\text{class},i}$ is the number of entries in \bar{y} of the same class as the i^{th} label entry (the class can be either 0 or 1 in our detection case) and f_m is the mean of $N_{\text{class}=0}$ and $N_{\text{class}=1}$.

When no human subjects are detected, the label map \bar{y} will only contain null values for long iteration periods, leading to the *over-fitting* of the system on this local context. We alleviate this problem by keeping Ψ *fixed* when no human subjects are present, and only enabling learning for Φ . In addition, we *prune* the task-driven contribution to the learning of Φ (22) for values of \mathcal{L}_{sup} smaller than a threshold $\theta_{th} = 0.2$ (empirically found to work well). Doing so, we avoid the over-fitting of the system by sporadically learning hard examples only.

Regarding the choice of the on-line optimizer for the convolutional readout, we choose the *Adam* optimizer [17] because of its adaptive gradient scaling capability, which, in an on-line learning setting, leads to faster convergence compared to SGD. In addition, the use of momentum in Adam implicitly incorporates gradients from the data in hind-side, re-balancing the learning process over time [17].

F. Post-processing

A set of discrete detections is obtained from the attention map as follows. First, a threshold d_{th} is applied to the map and a point cloud is formed. Then, a set of detected clusters $\{C_k\}$ is obtained by applying DBSCAN clustering [19] with *min points* = 2 and $\epsilon = 5$ (empirically tuned).

V. EXPERIMENTAL RESULTS

In this section, we assess the bio-inspired CL architecture described in Section IV on the *KUL-UAVSAFE* dataset [2] for people detection on drones. The *KUL-UAVSAFE* dataset features a collection of joint DVS and RGB acquisitions in an *indoor*, industrial-like environment, where a human subject is walking randomly. During our experiments, we choose the three longest acquisitions (~ 2 min.) from the *f-wall* collection in [2], where the drone and a human subject are moving in a space surrounded by walls, benches and shelves (different human subjects are featured to add variability).

We assess the performance of our system via 3-fold cross-validation as follows. First, one of the acquisitions is used as a *learning sequence* and is shown to our CL system *only once*, in its natural order (the learning sequence is *not shuffled*). Then, learning is stopped and a *different acquisition* is used to measure the *precision-recall* curves after post-processing (Section IV-F), by sweeping d_{th} from 0 to 1 and measuring the number of false alarms, true positives and false negatives in $\{C_k\}$. This process is repeated three times using different learning and testing sets and the final precision-recall curves are obtained as the average over the three learn-test folds.

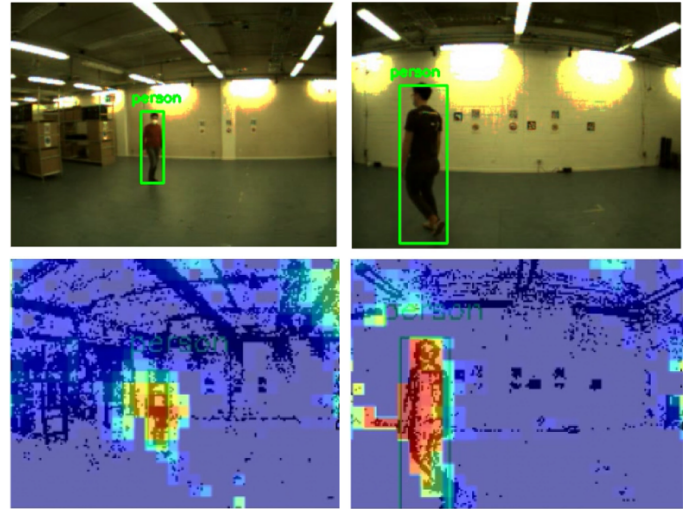


Fig. 6: **Attention maps** inferred from the DVS data by our bio-inspired CL SNN-STDP system. An off-the-shelve YOLOv3 is used for online labelling.

Fig. 6 shows examples of attention maps produced by our system. Table I reports the SNN-STDP learning parameters (found empirically, starting from the parameter set used in [12]). Table II reports the parameters used in our system architecture (tuned empirically). For the readout, we use the default values of the Adam optimizer [17] with a learning rate $\eta_r = 5 \times 10^{-6}$. Next, we will study the effect of the most important parameters impacting the CL procedure: the focal loss parameter γ (17) and the semi-supervision hyper-parameters $\lambda_{u,s}$ (16).

A. Impact of the focal loss parameter γ

We explore the impact of γ in (17) by keeping all other parameters constant with $\lambda_u = 0$, $\lambda_s = 1$. Fig. 7 shows the

| η_1 | η_2 | μ_1 | τ_m | λ_2 | A_+ | A_- | τ_+ | τ_- | τ_s |
|----------|----------|---------|----------|-------------|-------|-------|----------|----------|----------|
| 0.07 | 0.05 | 0.15 | 0.07 | 0.002 | 1 | 0.8 | 0.02 | 0.008 | 0.01 |

TABLE I: **SNN-STDP learning parameters.** The simulation time step is 0.005s. All τ values are in seconds. λ_1 in (16) is implicitly set by the neuron threshold μ [12]. $\theta_{th} = 0.2$. The negative STDP parameters are $A_{+,-}^n = A_{+,-}/100$.

| H | W | $l_{x,y}$ | d | M | $r_{x,y}$ | D_x | D_y |
|-----|-----|-----------|-----|-----|-----------|-------|-------|
| 130 | 173 | 30 | 5 | 64 | 12 | 21 | 29 |

TABLE II: **Architectural parameters.** $H \times W$: input size. $l_x \times l_y$: SNN kernel size, d : SNN stride, M : number of SNN kernels (neurons in the coding layer), $r_x \times r_y$: kernel size of the readout. $D_x \times D_y$: shape of the output attention map. The readout has a stride of 1 and zero-padding.

measured precision-recall curves. Fig. 7 also reports the peak F_1 score as $\max_i \frac{2P_i R_i}{P_i + R_i}$ along each precision-recall curve (P_i, R_i) [2]. Fig. 7 shows that the peak F_1 score is maximised near $\gamma = 0.5$. Therefore, $\gamma = 0.5$ in our experiments below.

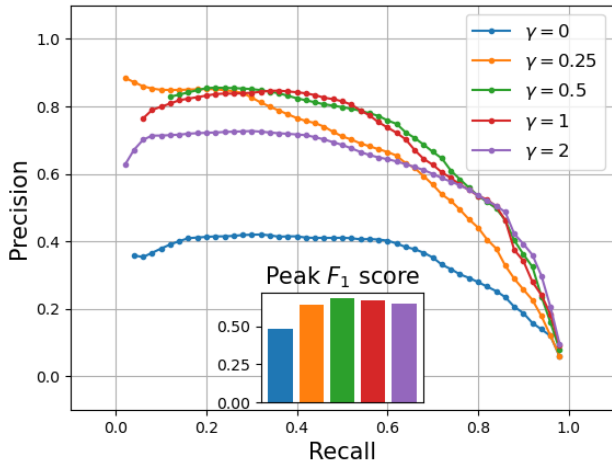


Fig. 7: **Impact of the focal loss parameter γ .** The peak F_1 score is maximized near $\gamma = 0.5$.

B. Impact of the unsupervised and supervised strengths λ_u, λ_s

Fig. 8 shows the precision-recall curves obtained by varying the *unsupervised* (negative STDP) and *supervised* contributions $\lambda_{u,s}$ in (16). Fig. 8 shows that the peak F_1 score is maximised near $\lambda_u = 0.2, \lambda_s = 0.8$. During our experiments, we also tried the use of the standard *positive* STDP rule for the unsupervised contribution, but always reached lower performances by varying λ_u , due to an increase in false alarms. In contrast, the use of the *negative* STDP rule for the *unsupervised* contribution provides an *opposite weight-steering force* to the *positive* STDP rule used for the *supervised* contribution, preventing the over-fitting of the system to structures in the environment. This leads to less false alarms at *higher recalls* and therefore, a higher detection performance (a non-trivial gain of +5% on the peak F_1 score vs. $\lambda_u = 0, \lambda_s = 1$).

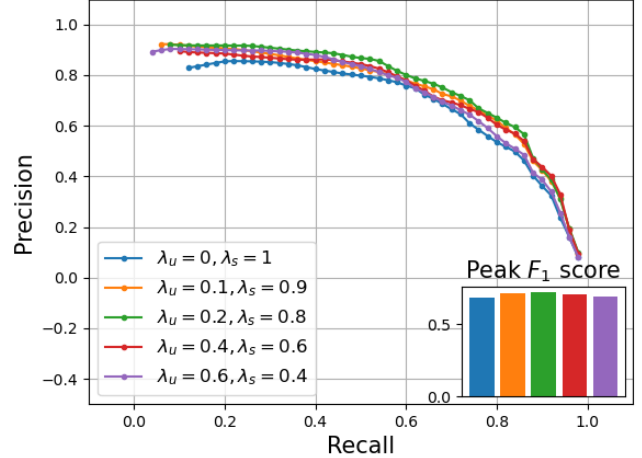


Fig. 8: **Varying the semi-supervised hyper-parameters $\lambda_{u,s}$.** The peak F_1 score is maximized near $\lambda_u = 0.2$ and $\lambda_s = 0.8$.

C. Continual SNN-STDP vs. standard CNNs

Since CNNs constitute the *standard approach* used in the vision pipelines of drones [4], we compare in Fig. 9 the performance of our CL architecture to two offline-trained CNNs: a SqueezeNet-based CNN trained with RGB data and a second SqueezeNet trained with *DVS frames* following [2] (DVS data averaged over time into frames at 30 FPS).

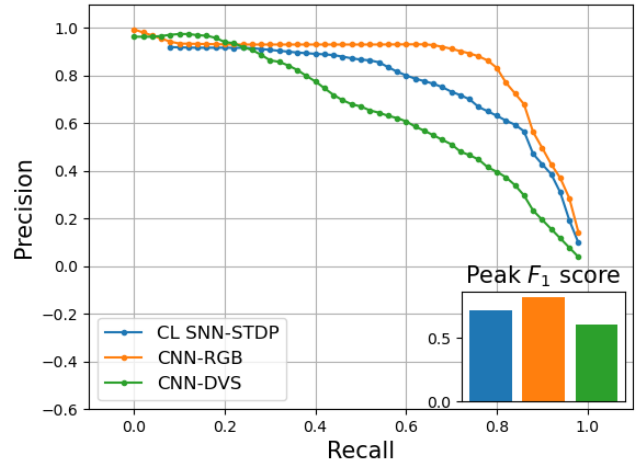


Fig. 9: **Detection precision vs. recall for the presented CL SNN-STDP and the conventional CNNs with offline training.**

Using a SqueezeNet CNN architecture is an appropriate choice for comparison since SqueezeNet aims to be MCU-friendly, using ~ 500 KB of weight memory (comparable to our network that uses 514KB). In order to *fairly* compare the bounding box output of the CNN to the attention map of our SNN-STDP system, we consider the image region delimited by the bounding box as the active region of an attention map (region inside the bounding box is filled with 1 and outside is filled with 0). We can then use the same precision-recall

measurement pipeline as used for the SNN. Fig. 9 shows that the CNN-RGB setup is the best performer (due to less false alarms compared to our SNN), but this comes at the cost of *on-line adaptability*. Indeed, the CNN has been trained offline for a specific environment and needs re-training each time new situations are encountered. This is in contrast to our CL SNN-STDP system which can learn and adapt on the fly, as demonstrated in this work. Interestingly, the CNN-DVS setup is the lowest performer and is significantly outperformed by the CL SNN-STDP system (+19% on the peak F_1 score). This is mainly due to the fact that the SNN introduces *time recurrence* through its lateral weights, enabling the network to learn *temporal features* that are neglected by the feed-forward CNN-DVS (see [18] for a discussion on temporal features in DVS data). This clearly shows the effectiveness of the methods proposed in Section IV for the continual learning of DVS data.

VI. CONCLUSION

This paper has presented, to the best of our knowledge, the first continual learning system for drones that learns to detect people on the fly using a bio-inspired SNN architecture with STDP learning. After the introduction of our novel methods, numerous experiments have been described to characterize the performance of our system and compare it against conventional CNNs. We have shown that our event-based system reaches a higher peak F_1 score (+19%) compared to a same-size CNN processing DVS frames, while enabling on-line adaptation and learning on the fly. As future work, we plan to increase the precision of the system at higher recalls by studying how to enhance the SNN expressivity with more layers and reducing false alarms. We hope that this work will inspire future research in brain-inspired vision for robotics.

ACKNOWLEDGMENT

We thank Lars Keuninckx and Tim Verbelen for their precious help. The research leading to these results has received funding from the Flemish Government (AI Research Program) and the European Union's ECSEL Joint Undertaking under grant agreement n° 826655 - project TEMPO.

REFERENCES

- [1] D. Falanga, K. Kleber, S. Mintchev, D. Floreano and D. Scaramuzza, "The Foldable Drone: A Morphing Quadrotor That Can Squeeze and Fly," in IEEE Robotics and Automation Letters, vol. 4, no. 2, pp. 209-216, April 2019, doi: 10.1109/LRA.2018.2885575.
- [2] A. Safa, T. Verbelen, I. Ocket, A. Bourdoux, F. Catthoor and G. E. Gielen, "Fail-Safe Human Detection for Drones Using a Multi-Modal Curriculum Learning Approach," in IEEE Robotics and Automation Letters, vol. 7, no. 1, pp. 303-310, Jan. 2022, doi: 10.1109/LRA.2021.3125450.
- [3] W. Fang, L. Wang and P. Ren, "Tinier-YOLO: A Real-Time Object Detection Method for Constrained Environments," in IEEE Access, vol. 8, pp. 1935-1944, 2020, doi: 10.1109/ACCESS.2019.2961959.
- [4] D. Palossi, A. Loquercio, F. Conti, E. Flamand, D. Scaramuzza and L. Benini, "A 64-mW DNN-Based Visual Navigation Engine for Autonomous Nano-Drones," in IEEE Internet of Things Journal, vol. 6, no. 5, pp. 8357-8371, Oct. 2019, doi: 10.1109/JIOT.2019.2917066.
- [5] J. Redmon, A. Farhadi. (2018). "YOLOv3: An Incremental Improvement."
- [6] A. Vitale, A. Renner, C. Nauer, D. Scaramuzza and Y. Sandamirskaya, "Event-driven Vision and Control for UAVs on a Neuromorphic Chip," 2021 IEEE International Conference on Robotics and Automation (ICRA), 2021, pp. 103-109, doi: 10.1109/ICRA48506.2021.9560881.

- [7] A. Mitrokhin, C. Fermüller, C. Parameshwara and Y. Aloimonos, "Event-Based Moving Object Detection and Tracking," 2018 IEEE/RSJ International Conference on Intelligent Robots and Systems (IROS), 2018, pp. 1-9, doi: 10.1109/IROS.2018.8593805.
- [8] Bi, G.q., Poo, M.m. (1998). Synaptic Modifications in Cultured Hippocampal Neurons: Dependence on Spike Timing, Synaptic Strength, and Postsynaptic Cell Type. Journal of Neuroscience, 18(24), 10464-10472.
- [9] C. Frenkel, M. Lefebvre, J. -D. Legat and D. Bol, "A 0.086-mm² 12.7-pJ/SOP 64k-Synapse 256-Neuron Online-Learning Digital Spiking Neuromorphic Processor in 28-nm CMOS," in IEEE Transactions on Biomedical Circuits and Systems, vol. 13, no. 1, pp. 145-158, Feb. 2019, doi: 10.1109/TBCAS.2018.2880425.
- [10] G. Gallego et al., "Event-based Vision: A Survey," in IEEE Transactions on Pattern Analysis and Machine Intelligence, doi: 10.1109/TPAMI.2020.3008413.
- [11] A. J. Ijspeert (2008). "Central pattern generators for locomotion control in animals and robots: A review." Neural Networks, 21(4), 642-653.
- [12] Ali Safa et al., (2021). "Learning Event-based Spatio-Temporal Feature Descriptors via Local Synaptic Plasticity: A Biologically-Plausible Perspective of Computer Vision." (<https://arxiv.org/abs/2111.00791>), Submitted to IEEE Transaction on Neural Networks and Learning Systems.
- [13] T. Hu, C. Pehlevan and D. B. Chklovskii, "A Hebbian/Anti-Hebbian network for online sparse dictionary learning derived from symmetric matrix factorization," 2014 48th Asilomar Conference on Signals, Systems and Computers, 2014, pp. 613-619, doi: 10.1109/ACSSC.2014.7094519.
- [14] Ioffe, S. et al., (2015). "Batch Normalization: Accelerating Deep Network Training by Reducing Internal Covariate Shift." In Proceedings of the 32nd International Conference on Machine Learning (pp. 448-456).
- [15] T. -Y. Lin, P. Goyal, R. Girshick, K. He and P. Dollár, "Focal Loss for Dense Object Detection," in IEEE Transactions on Pattern Analysis and Machine Intelligence, vol. 42, no. 2, pp. 318-327, 1 Feb. 2020, doi: 10.1109/TPAMI.2018.2858826.
- [16] D. Eigen and R. Fergus, "Predicting Depth, Surface Normals and Semantic Labels with a Common Multi-scale Convolutional Architecture," 2015 IEEE International Conference on Computer Vision (ICCV), 2015, pp. 2650-2658, doi: 10.1109/ICCV.2015.304.
- [17] Diederik P. Kingma, Jimmy Ba. (2017). "Adam: A Method for Stochastic Optimization."
- [18] X. Lagorce, G. Orchard, F. Galluppi, B. E. Shi and R. B. Benosman, "HOTS: A Hierarchy of Event-Based Time-Surfaces for Pattern Recognition," in IEEE Transactions on Pattern Analysis and Machine Intelligence, vol. 39, no. 7, pp. 1346-1359, 1 July 2017, doi: 10.1109/TPAMI.2016.2574707.
- [19] Ester, M., Kriegel, H.P., Sander, J., Xu, X. (1996). "A Density-Based Algorithm for Discovering Clusters in Large Spatial Databases with Noise." In Proceedings of the Second International Conference on Knowledge Discovery and Data Mining (pp. 226-231). AAAI Press.